The Astrophysical Journal Letters, 811:L9 (6pp), 2015 September 20 doi:10.1088/2041-8205/811/1/L9

COMPARATIVE MORPHOLOGY OF SOLAR RELATIVISTIC PARTICLE EVENTS

Leon Kocharov[1], Andreas Klassen[2], Eino Valtonen[3], Ilya Usoskin[1,4], and James M. Ryan[5]
[1] Sodankylä Geophysical Observatory (Oulu Unit), P.O.B. 3000, University of Oulu, FI-90014 Oulu, Finland
[2] Institut für Experimentelle und Angewandte Physik, Christian-Albrechts-Universität, D-24118 Kiel, Germany
[3] Department of Physics and Astronomy, University of Turku, FI-20014 Turku, Finland
[4] Department of Physics, University of Oulu, FI-90014 Oulu, Finland
[5] Space Science Center, Institute for the Study of Earth, Oceans and Space, University of New Hampshire, Durham, NH 03824, USA
Received 2015 July 28; accepted 2015 August 27; published 2015 September 17

ABSTRACT

Time profiles of the 0.25–10 MeV electrons and the $\sim$(0.1–1) GeV nucleon^{-1} protons and helium associated with two solar coronal mass ejections (CMEs) are analyzed with a newly formulated method based on modeling of the particle transport in the interplanetary medium. With the modeling, we fit the observed angular distribution of solar particles and infer, for a particular particle instrument and magnetic field orientation, the time delay of the particle registration at 1 AU in respect to the solar source. Then, after the time offset removal, intensity re-normalization and background equalization, the time–intensity profiles of high-energy protons, helium and electrons in different energy channels are superposed and compared. The comparison reveals episodes of remarkable coincidence of different profiles, as well as episodes of essentially different behavior. It implies at least three sources of solar high-energy particles operating in a single event. The first, short-duration source emits electrons next to the flare's impulsive phase and CME liftoff. The second source gradually rises and continues for more than an hour, emitting electrons and lower energy protons, which is consistent with shock acceleration on open magnetic field lines extending to solar wind. An another, third source is the main source of relativistic ions in space. It is retarded in respect to the flare's impulsive phase and may be associated with a structure encountered by the shock within a few solar radii from the Sun.

Key words: acceleration of particles – shock waves – Sun: corona – Sun: coronal mass ejections (CMEs) – Sun: flares – Sun: particle emission

1. INTRODUCTION

Solar energetic particle (SEP) events basically comprise two main classes—weak, impulsive events and major, gradual events (e.g., Cane & Lario 2006 and references therein). In an extreme case of gradual events, solar protons are accelerated to the energy $\gtrsim$1 GeV and thus can cause a signal in the ground-based neutron monitors, referred to as ground level enhancement (GLE; e.g., Gopalswamy et al. 2012). A typical GLE consists of a prompt component and a delayed component, which are distinct in terms of the proton energy spectrum, flux anisotropy, and width of their spread over the heliolongitude (Klein et al. 2014; Moraal & Caballero-Lopez 2014 and references therein).

The SEP events are typically ascribed either to solar flares or to coronal mass ejections (CMEs; e.g., the recent work by Kim et al. 2014). An association of SEPs with possible progenitors on the Sun is often based on the registration time of the first particles distinguishable above the actual background (Cane & Lario 2006). This is a "heritage" of the flare particle paradigm, in which SEPs were thought to be impulsively emitted from the Sun (for a historical review, see Cliver 2009). While the first particle timing is important, a background-dependent instant of time may be a poor proxy for the prolonged process of SEP emission in gradual events. Alternatively, one can fit with an SEP transport modeling the observed time profiles of the particle flux and anisotropy at 1 AU, and thus infer the SEP source profile at the Sun (e.g., Kocharov et al. 2010). However, actual SEP events may be very complicated, so their fitting should be done on a case-by-case basis, which especially hampers statistical studies.

In this Letter, as a compromise, we propose a method that also employs the SEP anisotropy data and modeling but allows faster analysis and comparison of numerous profiles in their entire complexity, with a focus on the prolonged emission of high-energy particles in extreme solar events.

2. DATA AND METHOD

We use the proton, helium, and electron data from the particle instrument Energetic and Relativistic Nuclei and Electrons (ERNE) and the Electron Proton Helium Instrument (EPHIN), both on the *Solar and Heliospheric Observatory* (*SOHO*) spacecraft (Müller-Mellin et al. 1995; Torsti et al. 1995). The High Energy Detector (HED) of ERNE can measure protons and helium in the energy range 12–140 MeV nucleon^{-1} with a good energy and angular resolution within the 120° full-width conical field of view, with its axis pointing in the ecliptic plane in the direction 45° from the spacecraft–Sun direction either to the west or to the east, depending on the flight schedule. The EPHIN instrument points in the same direction, with an 83° wide view cone, and is capable of measuring, among others, the 0.25–10 MeV electrons. In major events, however, the proton channels of ERNE may be overloaded. In such a case, we supplement ERNE data with data of the *GOES* proton channel P6 (80–165 MeV). In extreme solar events, high-energy nuclei also can be registered by the worldwide network of neutron monitors. From the network data, one can infer the angular distribution and energy spectrum of $\gtrsim$400 MeV nucleon^{-1} ions (e.g., Mishev et al. 2014), but protons and helium cannot be separated. The ion identification in the high-energy range is possible with modern spaceborne instruments like PAMELA

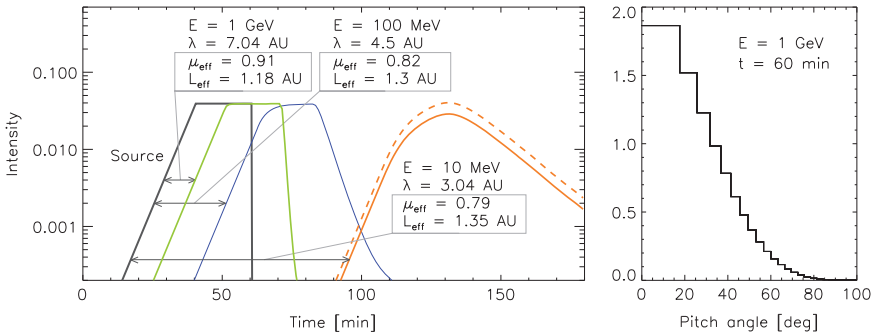

Figure 1. Simulated time–intensity profiles of 10 MeV, 100 MeV, and 1 GeV protons arriving at the Earth's orbit from the near-Sun source (left panel). Protons are registered within the ERNE/HED view cone. Interplanetary magnetic field makes the angle $\alpha_M = 60°$ with the axis of detector's view cone. Solar wind speed is 600 km s^{-1}. Solid profiles are normalized to the same value of time-integrated intensity. Dashed profile is alternatively normalized to the intensity maximum. Arrows indicate the time shifts of the 1 AU profiles. Similar shifts would result from a scatter-free propagation over the distance $L_{\rm eff}$, which corresponds to the mean pitch-angle–cosine value $\mu_{\rm eff}$. Right panel shows the pitch-angle distribution of 1 GeV protons at the event maximum. It is close to the angular distribution inferred from the neutron monitor observations of the 2006 December 13 GLE (Vashenyuk et al. 2008).

(Adriani et al. 2011) and AMS (Ting 2013), but due to low orbits, they suffer regular gaps in the SEP observations. Thus, we combine together the data of different detectors.

Observed particle intensities depend on the interplanetary transport from the near-Sun source to the detector at the Earth's orbit, as well as on the instrument's aperture angle and the viewing direction with respect to the interplanetary magnetic field. The particle scattering conditions in the solar wind are highly variable but can be estimated for a particular SEP event using the observed pitch-angle distributions. Around GLE maximum, the pitch-angle distribution may be very anisotropic, indicating the mean free path is well in excess of 1 AU. In such a case, the observed SEP rise profile is close to the profile of solar injection but shifted in time by $L_{\rm eff}/v$, where $L_{\rm eff}$ is the effective distance traveled by the particles of speed v. The traveled distance is longer than the length of the magnetic field line by a factor of $\mu_{\rm eff}^{-1}$, where $\mu_{\rm eff}$ is the pitch-angle cosine averaged over the trip of particles registered in the instrument's view cone. The time-shift values and the parameters $L_{\rm eff}$ and $\mu_{\rm eff}$ can be deduced with the SEP transport and registration modeling.

Interplanetary propagation of solar energetic protons is modeled in the framework of focused transport (similar to Kocharov et al. 2009) for the Kolmogorov turbulence spectrum in the standard solar wind, with the particle mean free path λ being independent of the heliocentric distance in the 0.1 AU vicinity of the Sun and linearly increasing with the magnetic field line length farther from the Sun (the mean free path values given in Figure 1 are for the Earth's orbit). The energy dependence of the proton mean free path is according to the standard quasi-linear theory, while the mean free path of $\approx$1 MeV electrons is equal to that of the 1 MeV protons (referring to Figure 8 by Bieber et al. 1994).

For the illustrative simulation of Figure 1, a mono-energetic proton source is placed at the heliocentric distance of $1.5R_\odot$, with the time profile shown in the figure. Simulated SEP distributions at the Earth's orbit are integrated over the instrument's view cone (with a flat response function inside the cone). In this example, the view-cone width is identical to that of the ERNE/HED and the instrument's axis faces 60° off the direction of interplanetary magnetic field. It is seen that at large values of the particle mean free path, $\lambda \gtrsim 3$ AU, the particle source profile may be estimated by a proper shifting of the instrument's counting-rate profile back in time, but a stronger scattering can blur the "image" of the source. For analysis of real events, we calculate the time shifts for the actual SEP energy spectrum, instrument's energy bandwidth, and viewing direction.

In order to make the time profiles of different particle registrations comparable, we shift each profile back to the Sun for the transport time and add 8.3 minutes for convenience of comparison with observed electromagnetic emissions: $t_s = t - \Delta t$, where $\Delta t = L_{\rm eff}/v - 8.3$ minutes, and $L_{\rm eff}$ comes from the modeling of a particular observation. As intensities of different particle species and energies may differ by orders of magnitude, we mutually re-normalize the observed time profiles to the same magnitude of a selected common feature, if such a feature is available.

Time profiles of different emissions may differ also in the signal-to-background level. The highest background level is in the neutron monitor counting rates. We reduce the neutron monitor background by subtracting 98%–99% of it to have the remnant background still not fluctuating too greatly in the logarithmic scale. Then, the background levels of other instruments are reduced to the remnant background of the neutron monitor by subtracting (or adding) some fraction of their actual background. Among tens of neutron monitors distributed all around the globe, we select one revealing the earliest onset and the steepest rise and consider its counting-rate profile as a proxy for the solar relativistic protons streaming along the interplanetary magnetic field. Thus, time profiles of different particle species and energies will be compared after the simulation-based time shifting, mutual re-normalization, and background equalization.

3. RESULTS

We illustrate the method with the analysis of two GLE–SEP events, 1998 May 2 (GLE 56; Figure 2) and 2006 December 13 (GLE 70; Figure 3). In the deka–MeV range, protons and helium were registered by *SOHO*/ERNE. The ERNE-observed proton pitch-angle distribution of the 1998 May 2 event was fitted with simulations of interplanetary transport by Kocharov et al. (2007). During the first hour of that event, the observed pitch-angle distribution corresponds to the proton mean free path $\lambda(20\,{\rm MeV}) = 18$ AU. Particle instruments on *SOHO* were facing off the magnetic field by the angle $\alpha_M \approx 75°$ (Figure 2(e)). These parameters are employed for estimating the time-shift values indicated in Figure 2. Panels (a)–(d) show

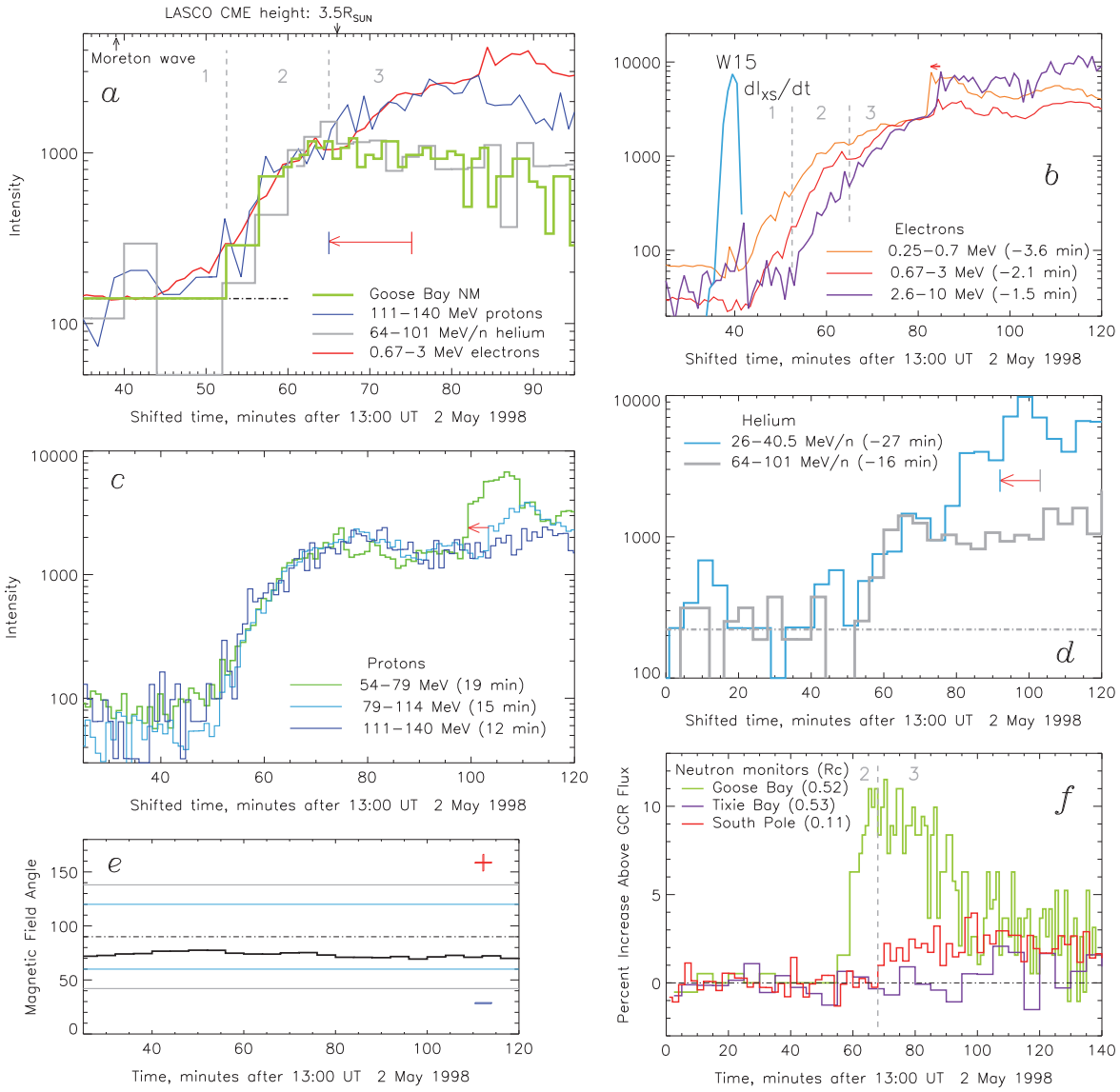

Figure 2. 1998 May 2 event. (a)–(d) Time-shifted and re-normalized SEP profiles of the 1998 May 2 event. The neutron monitor (NM) profile is shifted back by three minutes (a); time shifts of other profiles are indicated in the panels. Red arrows exemplify relative shifts in pairs of channels (in panels (b) and (c), the arrows are placed near selected features simultaneously occurring at 1 AU, like a jump in all electron channels at 80–85 minutes caused by an instrumental effect). In panel (a), 98.5% of the neutron monitor background is subtracted, while background levels of all other profiles are reduced to the remnant background of the neutron monitor (dashed–dotted line). Original background levels are kept in panels (b)–(d). (e) Angle α_M between the interplanetary magnetic field vector and the common axis of the *SOHO*/ERNE and *SOHO*/EPHIN view cones. Depending on the magnetic field direction, either toward (−) or away from (+) the Sun, the instrument view cones are situated either below or above the gray and blue lines for EPHIN and ERNE, correspondingly. In the beginning of this event, particles arrived anti-parallel to the magnetic field, and hence the negative magnetic polarity is applied. (f) Time profiles of several selected neutron monitors, with the entire background subtracted, not shifted, and not re-normalized. Geomagnetic cutoff rigidities of NMs (GV) are indicated. As a proxy of the flare's impulsive phase, we additionally plot in panel (b) the time derivative of the soft X-ray emission (0.05–0.3 nm; *GOES 9*). Also shown are the flare's longitude (b), the first observation of Moreton wave (Pohjolainen et al. 2001), and LASCO CME (a).

the observed SEP profiles as function of the shifted time $t_s = t - \Delta t(E)$.

We find a perfect coincidence of the proton profiles shown in Figure 2(c). Profiles are curved and thus could not coincide due to only re-normalization. The coincidence of time-shifted profiles indicates a simultaneous emission of different energies with no signature of possible acceleration dynamics. Also found is coincidence of the neutron monitor profile and profile of 64–101 MeV nucleon^{-1} helium (Figure 2(a)).

Three periods of particle emission can be selected (panel (a)). The middle period, Period 2, starts with the main rise of GLE nearly 10 minutes after the end of flare's impulsive phase and continues for about 15 minutes, until the start of the electron spectrum hardening evident from panel (b). In panel (a), the rise phase of the 111–140 MeV proton profile is normalized to the neutron monitor profile because they are of exactly the same shape within Period 2. The 0.67–3 MeV electron profile is normalized to protons, again because of the shape coincidence. The coinciding profiles (or segments) indicate the release of different particles from a common source operating in Period 2. This source is responsible for the prompt component of GLE. There are additional emissions before and after that period. Electrons below 3 MeV are emitted already in Period 1 (Figure 2(b)). In Period 3, a further rise is

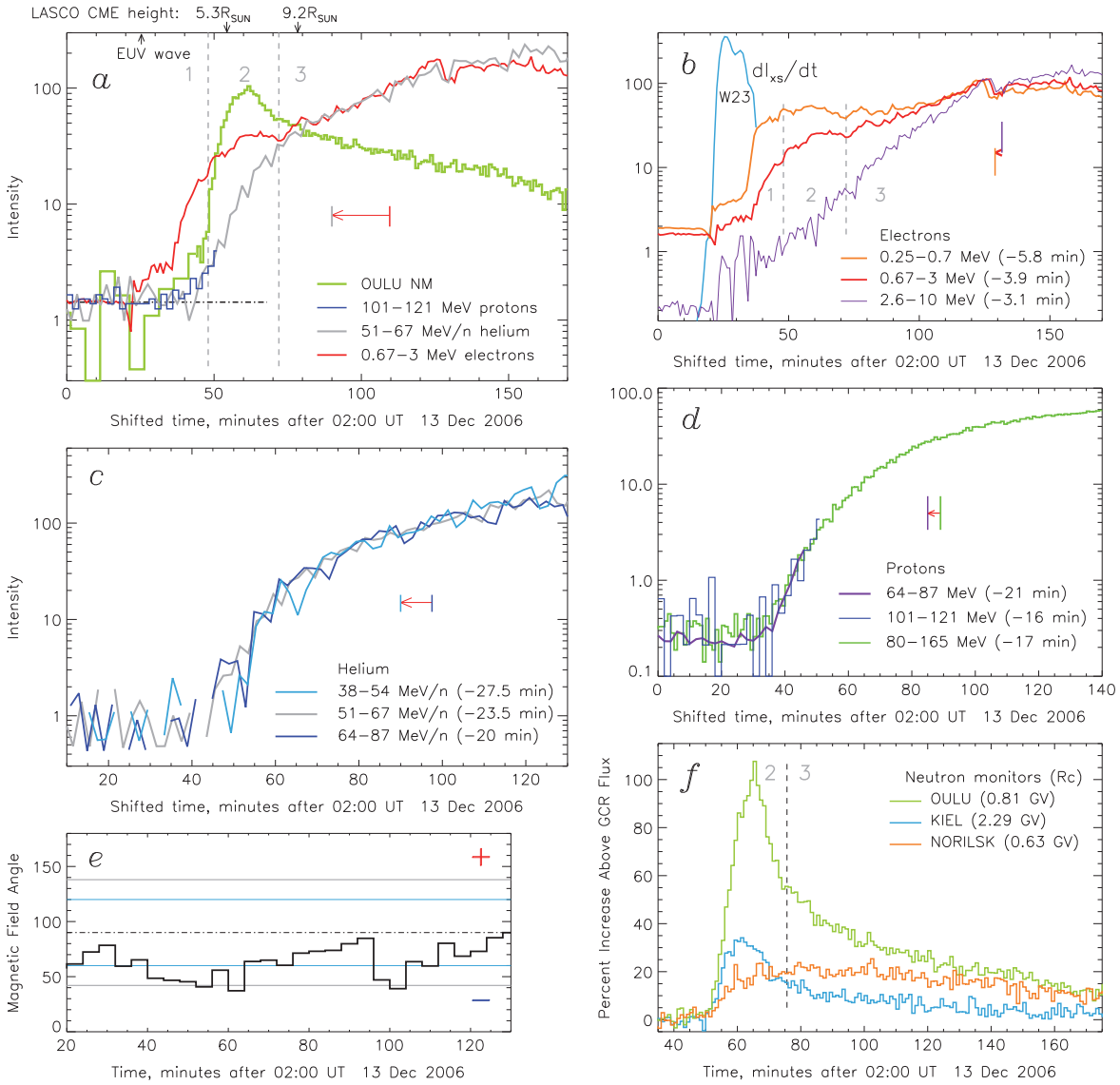

Figure 3. Same as in Figure 2, but for the SEP–GLE event of 2006 December 13. (a) Timing of the EUV wave is according to Miteva et al. (2014). (b) Employed X-ray data are from *GOES 10*. Enhancements in the electron channels during the flare's impulsive phase are contaminated by the hard X-rays. (d) The proton channel 80–165 MeV is P6 of *GOES 11*, while all other proton, helium, and electron channels are from *SOHO*.

seen in electrons and ≈100 MeV protons, while the high-energy helium and relativistic protons are already at the maximum (Figures 2(a) and (b)).

Pitch angle distribution of relativistic protons in GLE 70 (2006 December 13) was deduced by Vashenyuk et al. (2008) by fitting the neutron monitor network data. In our interplanetary transport model, such angular distribution corresponds to the mean free path $\lambda(1\,\mathrm{GeV}) = 7$ AU, and this value is used for estimating the time shifts $\Delta t(E)$, at the ERNE/EPHIN view-cone offset angle $\alpha_M = 60°$ (Figure 3(e)). The ERNE proton channels got overloaded shortly after the event start, but helium was accurately measured in three narrow channels between 38 and 87 MeV nucleon^{-1}. The helium profiles coincide after the preassigned time shifting (Figure 3(c)). The GLE main rise (start of Period 2) coincides with a steep rise of helium (Figure 3(a)). Period 2 ends with a change in the 0.67–3 MeV electron profile, where it joints the profile of helium, despite that they develop very differently before that.

Development of the helium abundance at ≈80 MeV nucleon^{-1} is additionally illustrated with Figure 4. For the He/p estimate, we use three helium channels of ERNE, while the time profile of 64–87 MeV proton intensity of ERNE is extrapolated to later times with the 80–165 MeV proton profile from *GOES 11* (Figure 3(d)). It is seen from Figure 4 that the main rise of the prompt component of GLE coincides with a new release of ≈80 MeV nucleon^{-1} helium without significant addition of ≈100 MeV protons so that the helium abundance jumps from $(\mathrm{He/p})_1 \approx 0.95\%$ up to $(\mathrm{He/p})_2 \approx 2.7\%$.

4. DISCUSSION

If the SEP flux anisotropy is high and the intensity rise in different energy channels reveals a velocity dispersion, the interplanetary transport bias can be corrected by shifting the observed count rate profile back in time. The particle flux anisotropy measurements and modeling of the interplanetary transport allow accurate estimation of the time delay between

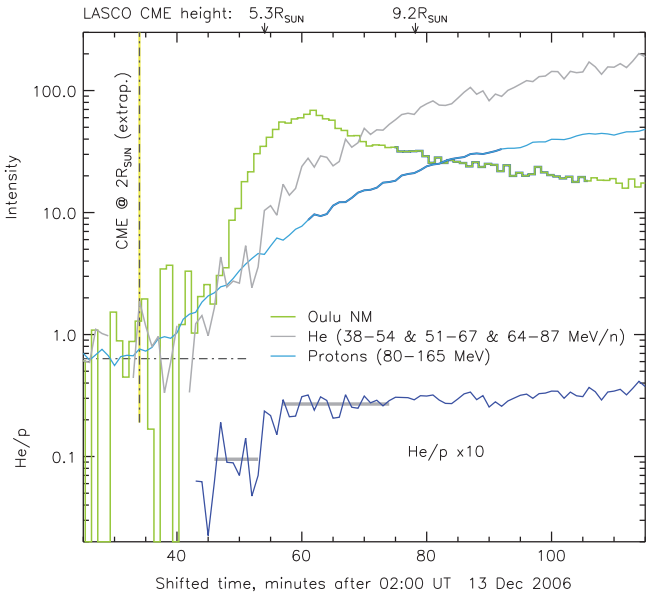

Figure 4. Helium-to-proton ratio during the 2006 December 13 event. Shown are the time-shifted and re-normalized profiles of the Oulu neutron monitor count rate, the proton channel P6 of *GOES 11*, and the average of three time-shifted profiles of helium from *SOHO*/ERNE. Background levels are equalized. The He/p profile (lowermost curve) is the ratio of the average of three helium channels of ERNE to the proton channel P6 of *GOES*, with backgrounds subtracted, normalized to the He/p ratio observed by ERNE in the 64–87 MeV nucleon^{-1} channel during t_s = 46–53 minutes, $(\mathrm{He/p})_1 = 0.95 \pm 0.25\%$. The helium abundance increases by factor of 2.8 ± 0.5 between the intervals of 46–53 and 57–74 minutes (horizontal gray bars). Additionally indicated are the (energy-dependent) periods of shifted time corresponding to the first period of PAMELA's observations, 03:18–03:49 UT (marked out by thickening of the neutron monitor and *GOES* profiles).

the solar source and the particle event in the instrument at 1 AU (Figure 1). In contrast to the traditional velocity dispersion analysis of the "first particle" registration time, the time-shifting technique operates with the entire rise profile, and hence does not depend on the background level over which a "first particle" of the gradually rising profile can be recognized.

Among all strongly anisotropic events of the *SOHO* era also well observed by the Oulu neutron monitor, we randomly pick two events. Being applied to these events, the analysis reveals more than one component of high-energy particles. Particle acceleration in gradual events is traditionally ascribed to the CME-driven shock acceleration on open magnetic field lines extending from the Sun to the Earth's orbit. The shock acceleration is expected to produce a single, smooth, and prolonged profile of the particle emission, and we find such patterns in Figure 3. In panel (b), the 2.6–10 MeV electron profile starts next to the flare's impulsive phase and smoothly continues for more than an hour. The same is valid for the ≈100 MeV protons in panel (d). The prolonged acceleration starts simultaneously with a pulse of the 0.25–3 MeV electron emission of Period 1 that may be counted as Source 1 (Figure 3(b)). The prolonged source, referred to as Source 2, starts simultaneously with Source 1 in Period 1 and proceeds through Period 3. These two sources should be complemented with a short-duration source operating only in Period 2 (Source 3) that is responsible for the prompt component of GLE (Figure 3(a)). Source 3 also significantly contributes to 38–87 MeV nucleon^{-1} helium and 0.25–3 MeV electrons. After Period 2, there is a new, joint rise of the electrons and helium. It may be ascribed either to one more source (like the extended coronal acceleration by Klein et al. 2014) or to the CME re-acceleration of previous components.

Extension of the prompt component of GLEs in heliolongitude is smaller than extension of the delayed component (e.g., Klein et al. 2014). Hence, it originates from a kind of core that is our Source 3. The core emission of the 2006 December 13 event is distinct also in the helium abundance (Figure 4). The event starts in Period 1 with prolonged emission from Source 2 with the He/p abundance ratio 0.95 ± 0.25%, which is typical for a gradual event. Then in Period 2, He/p jumps up to ≈2.7%. The nearly threefold rise of helium is not accompanied by a visible increase in protons. This implies that the abundance added by Source 3 should be rich in helium: He/p $\gtrsim$ 10%.

A part of the 2006 December 13 event was observed by the space spectrometer PAMELA in the energy range from ≈80 MeV nucleon^{-1} up to ≈3 GeV nucleon^{-1} (Adriani et al. 2011). The first time period of the PAMELA observation was 03:18–03:49 UT. Corresponding intervals of the shifted time are indicated with thick segments of the ≈100 MeV proton and neutron monitor profiles in our Figure 4. The PAMELA observed GeV nucleon^{-1} ions belong to the delayed component of GLE (Period 3), while ≈100 MeV nucleon^{-1} ions are partly from Period 2. At ≈80 MeV nucleon^{-1}, the He/p ratio observed by PAMELA coincides with our estimate: He/p ≈ 2.5% (Figure 5 of Adriani et al. 2011). However, PAMELA's range extends to GLE energies, and in the rigidity range 1.3–3 GV, the He/p abundance ratio is observed to be a constant close to 10% (Figure 7 of Adriani et al. 2011). Our Figure 4 suggests that the energy spectra of helium and protons observed by PAMELA are sampled from at least two different sources differently weighted depending on the ion species and energy.

In the considered events, neither of high-energy particle emissions directly come from the flare's impulsive phase, while the first peak of >0.25 MeV electrons observed in some other GLEs could be of the flare origin (Klassen et al. 2005). Irrespective to the timing of first particles, we find more than one source shaping each SEP event after the flare's impulsive phase. We also note episodes of identical shifted-time profiles of different particle species and energies, which may be explained by the particle release at opening of a magnetic trap. Even a single shock can produce a structured SEP source profile when propagating in a structured environment, which may include coronal/CME loops and/or streamers. For instance, Kocharov et al. (2015) recently considered a theoretical model of the shock acceleration of high-energy protons in a pre-existing turbulent ray, which could mimic the CME shock acceleration in a coronal streamer disturbed by previous CMEs or jets.

In conclusion, the morphological analysis of ∼(0.1–1) GeV nucleon^{-1} protons and helium and ∼(0.3–3) MeV electrons of the two SEP–GLE events associated with flares at heliolongitudes ∼20°W has revealed at least three particle sources: a short-duration source, which appears next to the flare and CME launch; a prolonged source, which is likely the CME shock on open magnetic field lines; and a late, short-duration source, Source 3, which is responsible for the prompt component of GLE and should be a compact structure left behind the shock within a few solar radii from the Sun.

We thank the *ACE*/MAG instrument team, the *ACE* Science Center, NOAA, and IZMIRAN for providing the data of *ACE*, *GOES*, and neutron monitors. *SOHO* is a project of international cooperation between ESA and NASA. Oulu neutron monitor data are available at http://cosmicrays.oulu.fi. This research was supported under grant 50 OC 1302 by the German DLR and by the Academy of Finland through projects 258963 and 260596.

REFERENCES

Adriani, O., Barbarino, G. C., Bazilevskaya, G. A., et al. 2011, ApJ, 742, 102
Bieber, J. W., Matthaeus, W. H., Smith, C. W., et al. 1994, ApJ, 420, 294
Cane, H. V., & Lario, D. 2006, SSRv, 123, 45
Cliver, E. W. 2009, in Proc. IAU Symp. 257, Universal Heliophysical Processes, ed. N. Gopalswamy & D. F. Webb (Cambridge: Cambridge Univ. Press), 401
Gopalswamy, N., Xie, H., Yashiro, S., et al. 2012, SSRv, 171, 23
Kim, R.-S., Cho, K.-S., Lee, J., Bong, S.-C., & Park, Y.-D. 2014, JGR, 119, 9419
Klassen, A., Krucker, S., Kunow, H., et al. 2005, JGR, 110, A09S04
Klein, K.-L., Masson, S., Bouratzis, C., et al. 2014, A&A, 572, A4
Kocharov, L., Laitinen, T., Vainio, R., et al. 2015, ApJ, 806, 80
Kocharov, L., Pizzo, V. J., Odstrcil, D., & Zwickl, R. D. 2009, JGR, 114, A05102
Kocharov, L., Reiner, M. J., Klassen, A., Thompson, B. J., & Valtonen, E. 2010, ApJ, 725, 2262
Kocharov, L., Saloniemi, O., Torsti, J., Kovaltsov, G., & Riihonen, E. 2007, ApJ, 654, 1121
Mishev, A. L., Kocharov, L. G., & Usoskin, I. G. 2014, JGR, 119, 670
Miteva, R., Klein, K.-L., Kienreich, I., et al. 2014, SoPh, 289, 2601
Moraal, H., & Caballero-Lopez, R. A. 2014, ApJ, 790, 154
Müller-Mellin, R., Kunow, H., Fleiβner, V., et al. 1995, SoPh, 162, 483
Pohjolainen, S., Maia, D., Pick, M., et al. 2001, ApJ, 556, 421
Ting, S. 2013, NuPhS, 243, 12
Torsti, J., Valtonen, E., Lumme, M., et al. 1995, SoPh, 162, 505
Vashenyuk, E. V., Balabin, Yu. V., Gvozdevsky, B. B., & Shchur, L. I. 2008, Ge&Ae, 48, 149